Crustal structure derived from seismic refractions and wide-angle reflections in the Mizuho Plateau, East Antarctica

Koji Yoshii[1][*][†], Kiyoshi Ito[1], Hiroki Miyamachi[2] and Masaki Kanao[3]

[1] *Disaster Prevention Research Institute, Kyoto University, Gokasyo, Uji 611-0011*
[2] *Faculty of Science, Kagoshima University, Kagoshima 890-0065*
[3] *National Institute of Polar Research, Kaga 1-chome, Itabashi-ku, Tokyo 173-8515*
[*] *Present address: Tokyo Electron Limited, 5–3–6, Akasaka, Minato-ku, Tokyo 107-8481*
[†] *Corresponding author. E-mail: yoshii@rolling.sun.net*

Abstract: Large seismic explosion experiments were conducted on the traverse route from Syowa to Mizuho Stations by the 41st Japanese Antarctic Research Expedition (JARE-41) in 1999–2000 and JARE-21 in 1980–1981. The *P*-wave velocity structure of the ice sheet, the crust and the uppermost mantle in the Mizuho Plateau, East Antarctica, is deduced from travel-time analysis of the combined data of refractions and wide-angle reflections. The ice sheet has a surface layer 60–100 m in thickness with *P*-wave velocity of 2.34–3.01 km/s, while the deeper part has a *P*-wave velocity of 3.80–3.85 km/s. There is a v-shaped valley with a drop of 600 m in the basement topography at the middle of the profile line; this is consistent with the variations of the ice-sheet flow. The uppermost crust has a *P*-wave velocity of 6.17–6.20 km/s on the coastal side, 6.08 km/s under the above mentioned v-shaped valley and 6.21–6.26 km/s on the inland side. The middle and the lower crustal *P*-wave velocities are 6.45 and 6.56 km/s, and their thicknesses are about 10 and 20 km, respectively. The Moho boundary is almost 40 km deep with a gentle dip toward the inland direction with a *Pn* velocity of 8.03 km/s. The *Vp/Vs* value of 1.70 for the entire crust is derived from *S*-wave travel-time analysis. Moreover, calculated gravity anomalies, based on the obtained velocity structure and a density-velocity relation obtained in the laboratory experiments, coincide well with observed anomalies, but there are some misfits at the v-shaped valley of the basement rock and around the S-1 and S-6 shot points at both ends of the profile. Compared with the results from high pressure laboratory measurements of velocities for metamorphic rocks, it is implied that felsic gneiss is possibly dominant in the uppermost crust along the Mizuho traverse route and that the basement layer with a *P*-wave velocity of 4.69 km/s near the coast and the v-shaped valley may be a mixture of ice with sand or stone.

key words: Mizuho Plateau, continental crust, refraction and reflection survey, *P*-wave velocity structure, Moho discontinuity

1. Introduction

Mizuho Plateau, in the eastern part of Dronning Maud Land, East Antarctica, was located in a breakup region of Gondwana, so it reveals important information about the structure of the crust and the uppermost mantle. In recent years, geological and

geophysical surveys have been conducted by the Japanese Antarctica Research Expeditions (JAREs) to study the structure and evolution of the East Antarctic lithosphere. The Mizuho Plateau area is considered to be a part of the Pan-African orogenic belts between Enderby Land and Dronning Maud Land (*e.g.*, Lawver *et al*., 1998; Harley and Hensen, 1990), and was connected with South India and Sri Lanka before the breakup of Gondwana in the mid-Mesozoic. After identifying the crustal structure and composition by our multidisciplinary interpretation, we can present a tectonic evolution model of the Mizuho area from the Pan-African orogeny until the present.

In the 1999–2000 austral summer, JARE-41 conducted a seismic experiment from the coast to inland along a profile 180 km long with a station spacing of 1 km on the Mizuho Plateau (Miyamachi *et al*., 2001). Figure 1 shows the profile lines. We can detect direct waves through ice sheets as well as refracted and reflected waves from the crust and the Moho discontinuity in the obtained record sections. Tsutsui *et al*. (2001a) presented a velocity structure of the ice sheet and the shallower part of the crust by the method of difference (Hagiwara, 1938) from the obtained data. However, they could not obtain the deep crustal structure, since the coverage of first arrivals is not long enough to derive the structure. Moreover, Tsutsui *et al*. (2001b) and Yamashita *et al*. (2002) analyzed reflected waves on the assumption of a simple velocity model without lateral velocity variations in the layers. However, when we can obtain a detailed velocity structure from the shallow to the deeper part of the crust, we can determine the
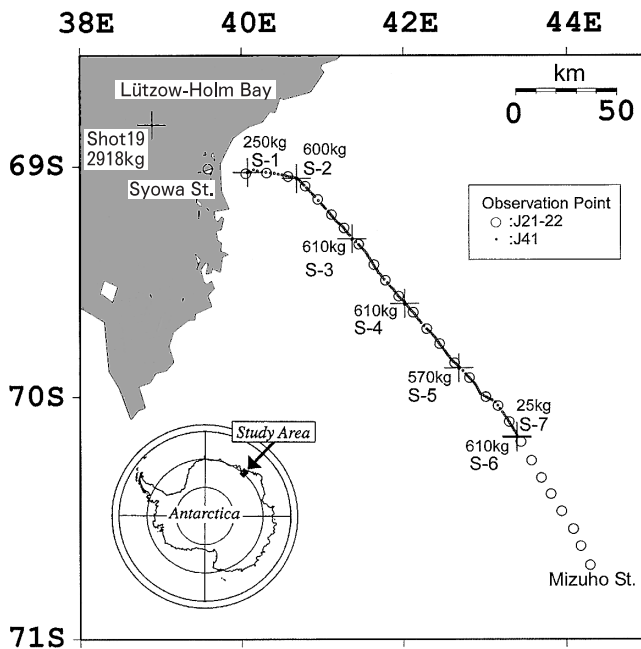

Fig. 1. *Map of shot points and observation stations. Shot 19 indicates the JARE-21 explosion and plus signs S-1 through S-7 are for the JARE-41 experiments. The charge sizes are also shown. The solid circles and open circles indicate the observation stations of the JARE-41 and JARE-21 experiments, respectively.*

more refined structure of the deeper part of the crust and upper mantle.

Previously, in the 1979–1981 austral summers, JARE-20, -21, and -22 conducted big seismic explosion experiments over a 300 km length on the same traverse routes (Ito *et al.*, 1983), with a relatively large station spacing of about 10 km. Seismograms from an explosion, fired at sea in Lützow-Holm Bay, showed especially clear refracted and reflected waves from the crust and the Moho boundaries. These travel-time data are good enough to reveal the deep structure of the crust. Therefore, we try to determine a more detailed *P*-wave velocity model from the analysis of combined data of these two experiments by using the technique of ray tracing. In addition, we analyze gravity data obtained along the same route to present a crustal density model. The theoretical gravity anomaly for the derived velocity structure was calculated on the basis of a relationship between seismic velocities and densities of rock obtained in the laboratory measurements. Further, we discuss the difference in rock types deduced from the velocities and densities, comparing with those for rocks from the laboratory experiments.

2.   Experiments and data

2.1.   JARE-41 experiment

JARE-41 conducted a seismic refraction and wide-angle reflection experiment with a high-density observation array along the Mizuho traverse route as described before (Miyamachi *et al.*, 2001). This experiment consisted of five large shots with dynamite of about 600 kg each and two small shots with charge sizes of 250 kg and 25 kg, respectively. The generated seismic waves were recorded with 160 recorders along a 180 km profile. In addition, at each shot point, 6–7 extra stations (near shot line-up stations) were installed with 100 m spacing to obtain velocities in the uppermost ice sheet. The locations of the shot points and the recording sites are shown in Fig. 1. A recording system for each station consisted of a vertical component seismometer with 2 Hz natural frequency and a digital data recorder at 200 Hz sampling. A clock with a quartz oscillator was embedded in the recorder and calibrated by a GPS receiver five times a day. The station locations were determined by GPS relative positioning.

For all shots, almost all stations worked well without problems and only a few stations failed to record the explosion waves. Arrival time data were picked up on non-filtered traces for refracted waves and on 2–16 Hz band-pass digital filtered traces for reflected waves; the pass-band was selected where the reflected waves were most clearly seen on the records. Figures 2 shows (a) original record sections and (b) a 2–16 Hz band-pass filtered record section for the shot S-1. For the shots from S-2 to S-7, similar record sections are obtained, as shown in Figs. 3–8, respectively. These record sections are characterized by two branches of arrivals, refracted waves from the ice sheet (*Pd*) and the crust (*Pg*). Clear waves reflected within the crust (*PiP* and *PiiP*) and from the Moho boundary (*PmP*) are also observed. The first branch of *Pg* refracted through the ice sheet has an apparent velocity of 3.8 km/s, and the second branch refracted through the crust, 6.2 km/s, respectively. An exceptional case is the record section for S-1 (Fig. 2), where the third branch with an apparent velocity of 4.7 km/s (*Px*) appears before the onset from 6.2 km/s. Another characteristic feature in

a)

A record section of S-1

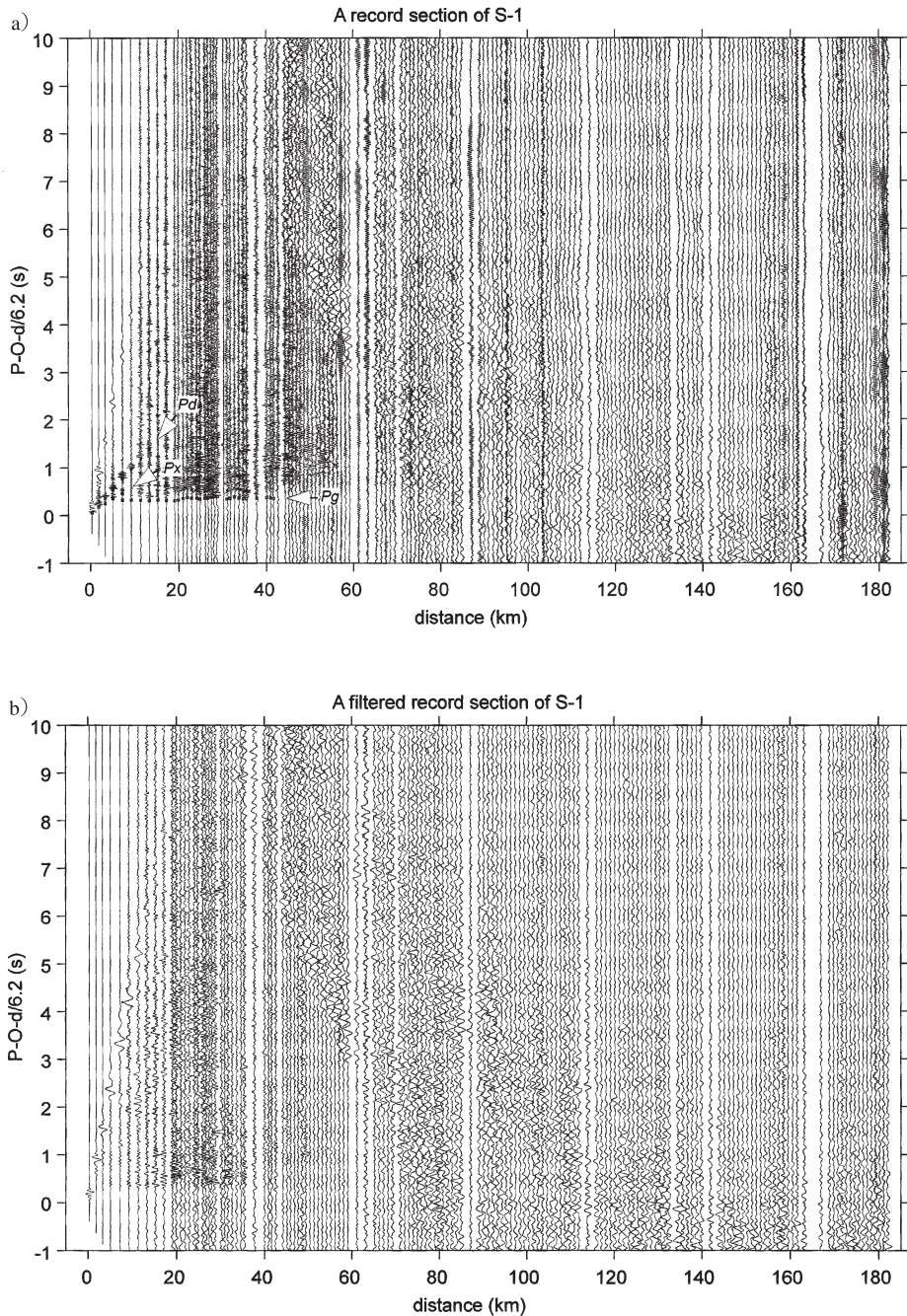b)

A filtered record section of S-1

Fig. 2. A record section for shot S-1, the onsets of refracted arrivals are marked by small squares. The abscissa shows the distance from the shot in km and the ordinate shows the reduced travel time in seconds with a reduction velocity of 6.2 km/s. Pd, Pg and Px indicate the refracted arrivals from the ice sheet, from the uppermost crust and from the layer with apparent velocity of 4.7 km/s, respectively.

a)

A record section of S-2

Pd

Pg

P-O-d/6.2 (s)

distance (km)

b)

A filtered record section of S-2
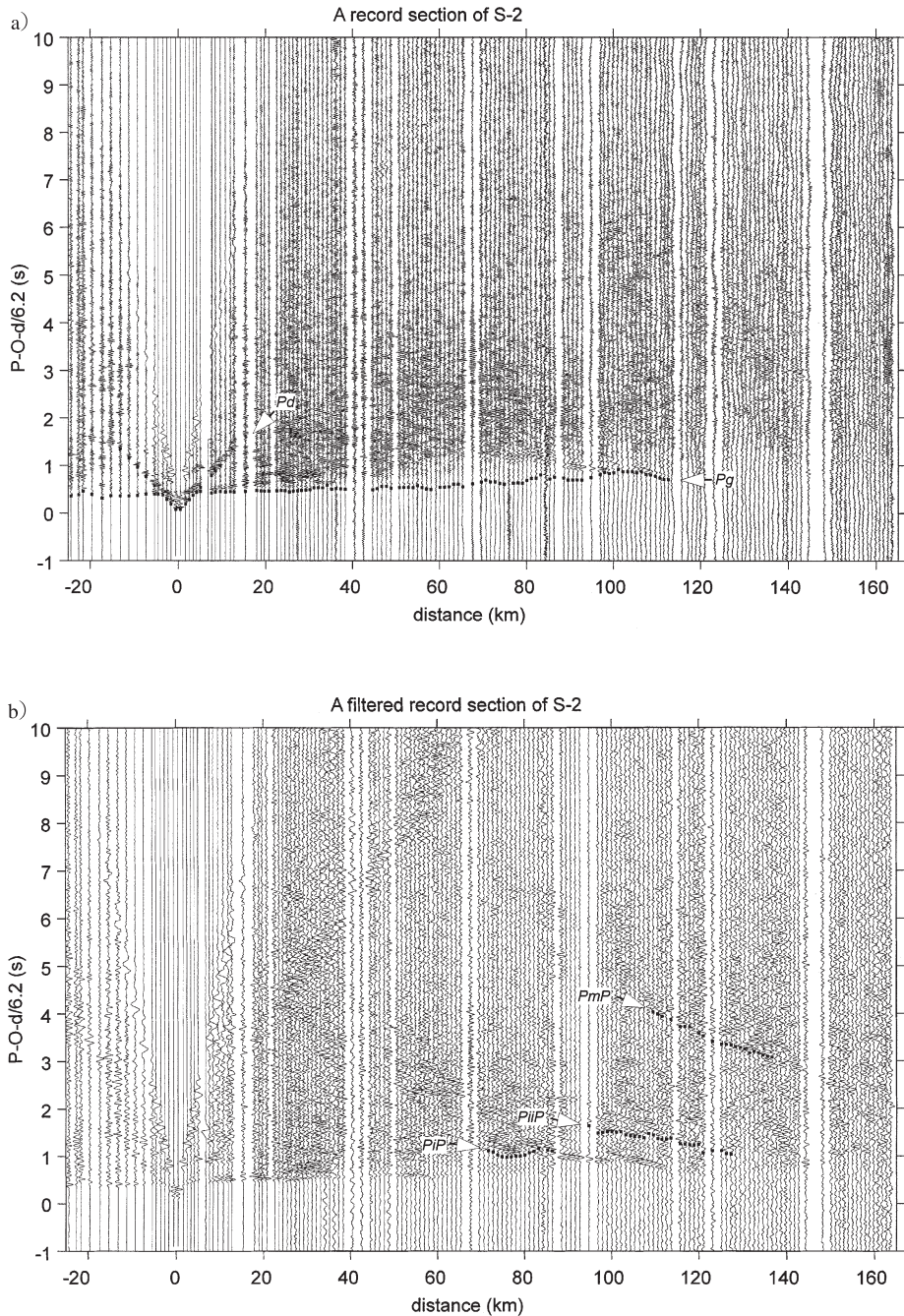
PmP

PiiP

PiP

P-O-d/6.2 (s)

distance (km)

Fig. 3. A record section for the shot S-2, (a) the onsets of refracted arrivals.   (b) A band-pass
filtered record (2–16 Hz) for the same shot.   Other than Pd and Pg, we see PiP, PiiP and
PmP, which indicate the reflected arrivals from the middle crust, lower crust and Moho
boundary, respectively.

a)

A record section of S-3
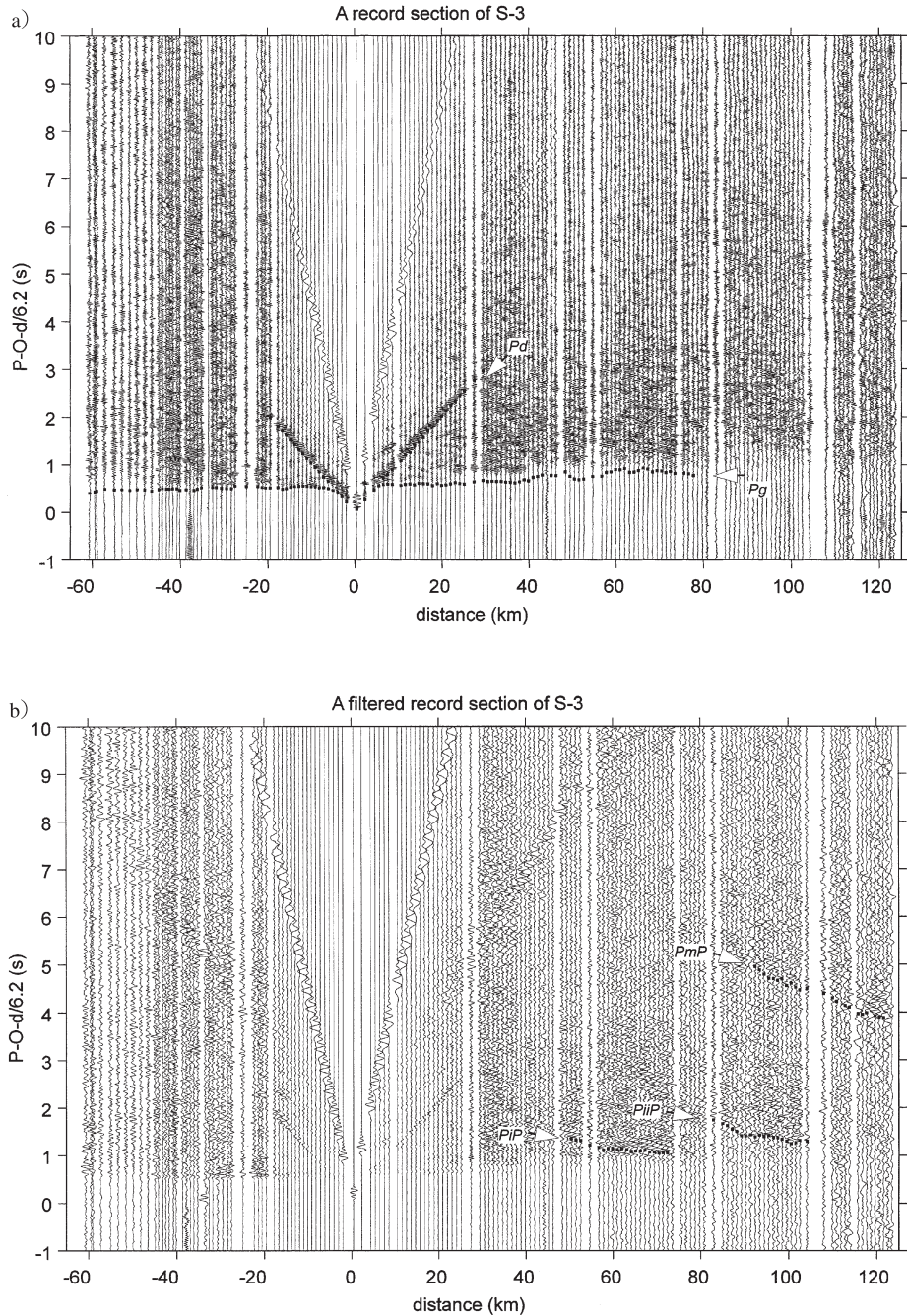

b)

A filtered record section of S-3

Fig. 4. A record section for shot S-3.   (a) refracted arrivals.   (b) A band-pass filtered record (2–16 Hz) for the same shot.   Explanations are the same as for Fig. 3.

a)

A record section of S-4

b)

A filtered record section of S-4

Fig. 5.   *A record section for shot S-4.   (a) refracted arrivals.   (b) A band-pass filtered record (2–16 Hz) for the same shot.   Explanations are the same as for Fig. 3.*
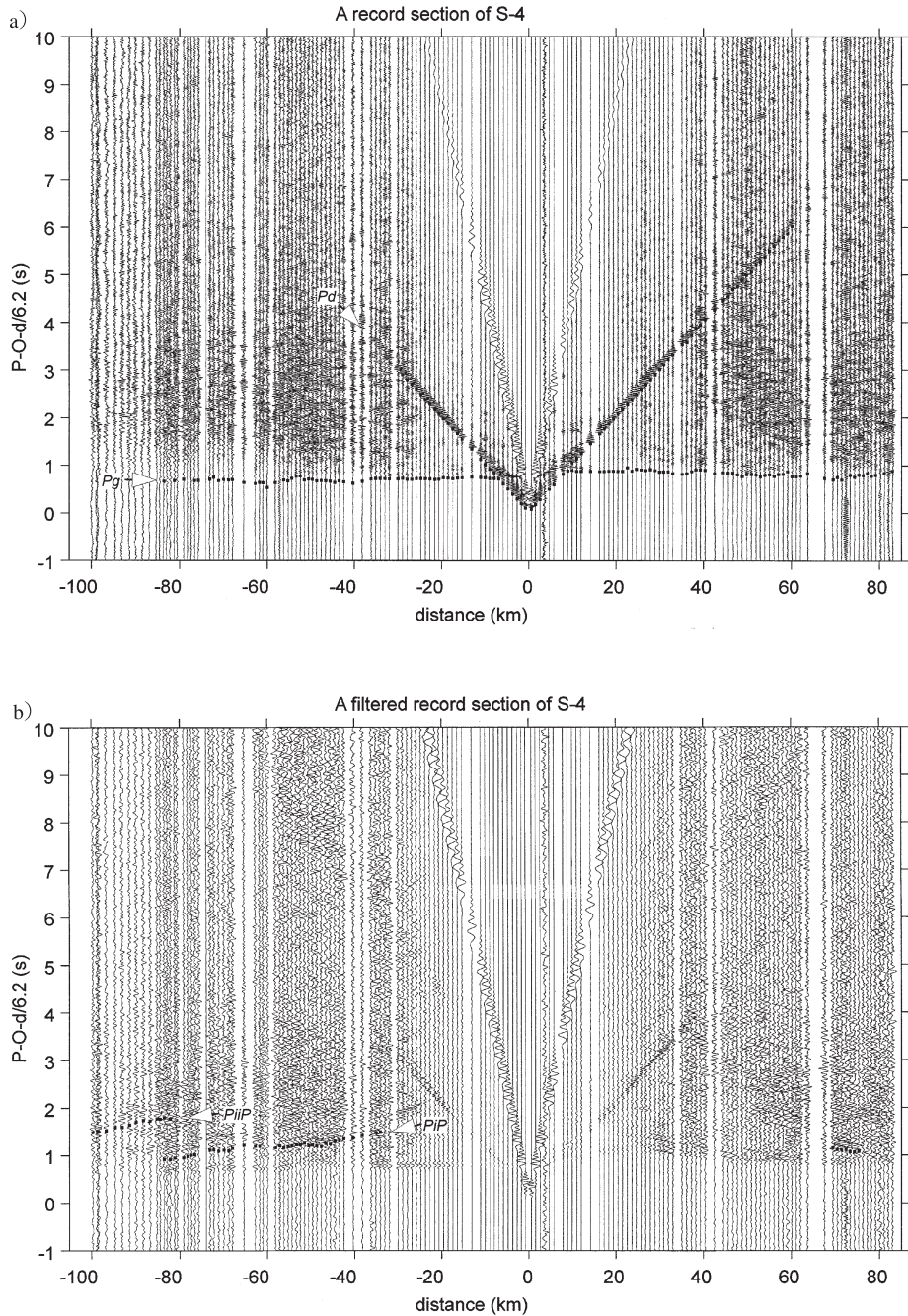
a)

A record section of S-5
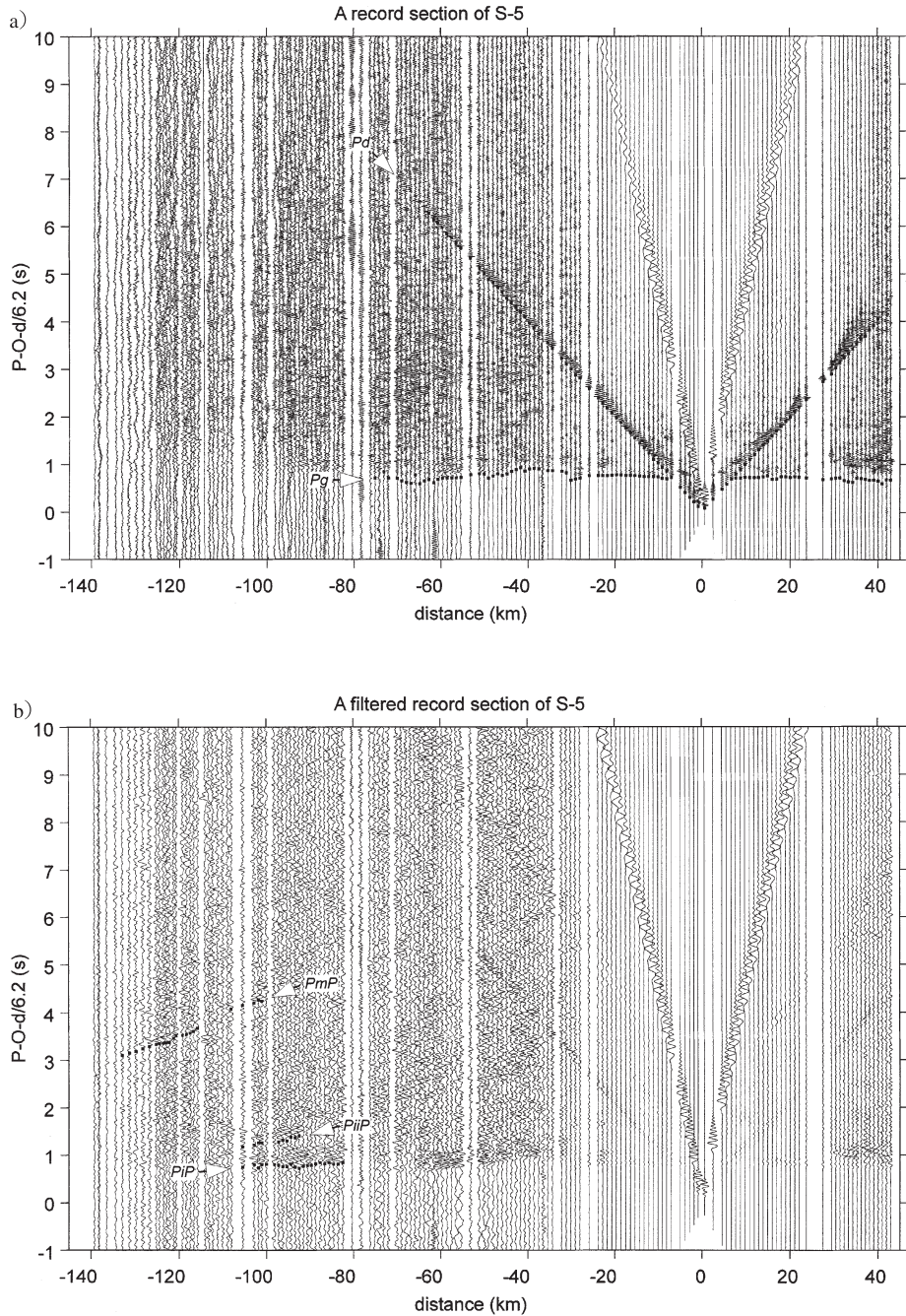

b)

A filtered record section of S-5

Fig. 6. A record section for shot S-5. (a) refracted arrivals. (b) A band-pass filtered record (2–16 Hz) for the same shot. Explanations are the same as for Fig. 3.

Fig. 7.   A record section for shot S-6.   (a) refracted arrivals.   (b) A band-pass filtered record (2–16 Hz) for the same shot.   Explanations are the same as for Fig. 3.
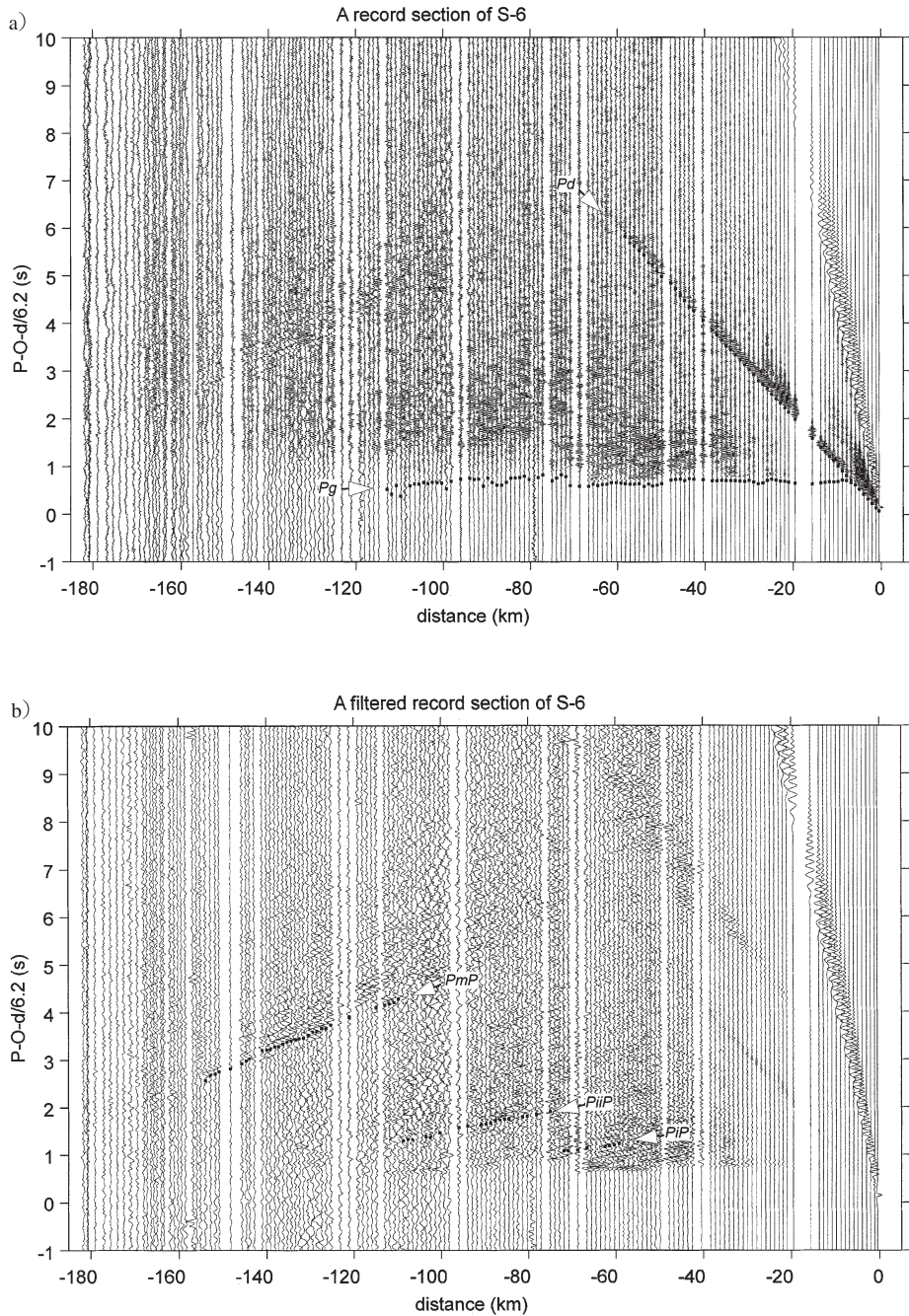
a)

A record section of S-7

b)

A filtered record section of S-7

Fig. 8.   A record section for shot S-7.   (a) refracted arrivals.   (b) A band-pass filtered record (2–16 Hz) for the same shot.   Explanations are the same as for Fig. 3.
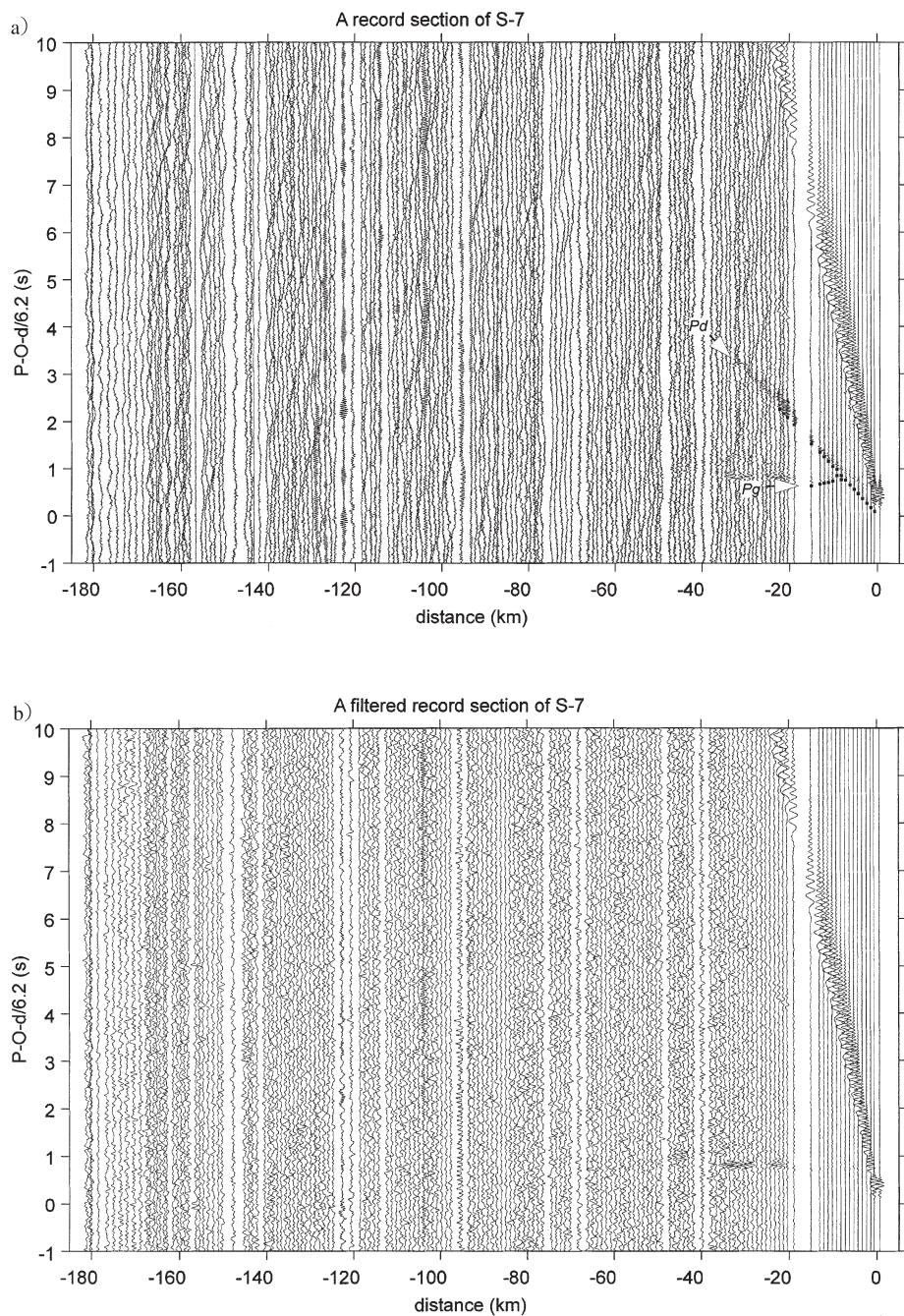
the record sections includes a large gap of intercept times by 0.3 s for 6.2 km/s travel times to opposite directions as shown in the record section for S-4 (Fig. 5). This gap indicates a large depression of the topography of the rock near the S-4 shot point.

Figure 9 shows first arrivals recorded at line-up stations for each shot from S-1 through S-7. Phases with apparent velocities of 2.5–3.0 km/s are observed up to the offset distance of 100–200 m and those of 3.64–3.73 km/s are observed at more distant stations as given by Miyamachi *et al.* (2001). These phases are followed by *Pd* phases with an apparent velocity of about 3.8 km/s, shown in Figs. 2a to 8a. This suggests that the ice sheet has a gradual velocity increase with depth.

Actually, there is evidence of continuous velocity increase from the previous experiment in 1968–1969. The JARE South Pole Traverse party undertook refraction experiments with five profiles of about 1 km, having station spacing of 20 m, which was shorter than those of the near-shot line-up observation by JARE-41. The analysis implied that the *P*-wave velocity continuously increased up to depth of 220 m in the upper transition zone from snow to ice (Eto, 1971). In addition, the bulk density variation with depth for drilled cores at Mizuho Station (Narita *et al.*, 1978), is consistent with that of *P*-wave velocity by Eto (1971). These surveys also suggest that the ice sheet has a continuous velocity increase with depth, a steeper increase near the
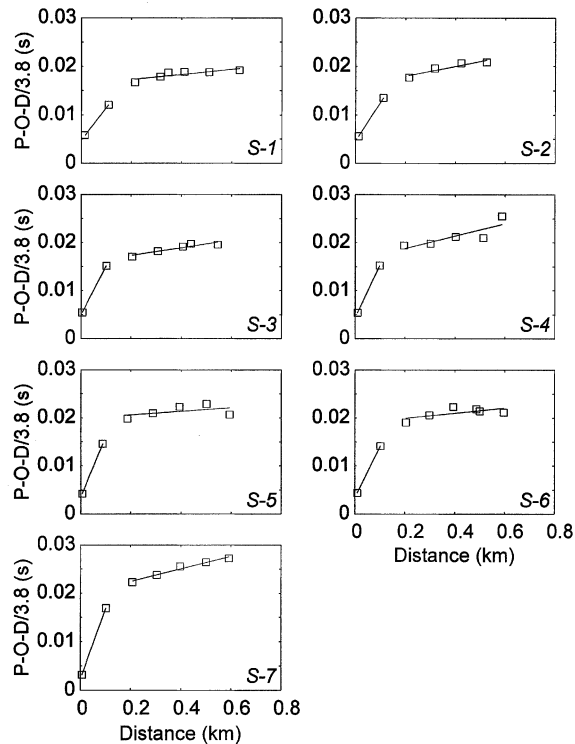

Fig. 9. *Travel time diagrams for the nearby shot line-up stations for each shot of the JARE-41 experiment. The abscissa shows the distance from the shot point in km and the ordinate shows the reduced travel time in seconds with a velocity of 3.8 km/s.*

surface and gradual one deeper than about 200 m.

2.2. JARE-21 and -22 experiments

JARE-20, -21 and -22 conducted seismic explosion experiments along the Mizuho traverse routes in 1979–1981 (Ito *et al.*, 1983).   These experiments consisted of three large shots with charge sizes of about 3000, 1400 and 1000 kg, respectively.   The generated seismic waves were recorded along a 300 km profile with 27 installed record-ers.   The location of the shot point (Shot 19) and the recording sites (open circles) are shown in Fig. 1.   The observation consisted of a vertical-component seismometer with 2 Hz natural frequency, a direct-analogue recording data-recorder and a high precision crystal clock (Ito *et al.*, 1983).   The clock was calibrated several times during the operation and station locations were determined with an NNSS (Navy Navigation Satellite System) receiver (Shibuya and Kaminuma, 1982; Shibuya *et al.*, 1982).

Seismograms of high-quality were obtained at all stations for Shot 19.   The seismograms were digitized at 100 Hz sampling and the arrival time data were picked up on non-filtered traces for all *P*-waves (Fig. 10).   The abscissa denotes distance from the shot point in km, while the ordinate axis denotes reduced travel-time with a velocity of 6.2 km/s.   The onsets of refracted and reflected waves from the crust and the Moho discontinuity are indicated by small square symbols.   This record section can be
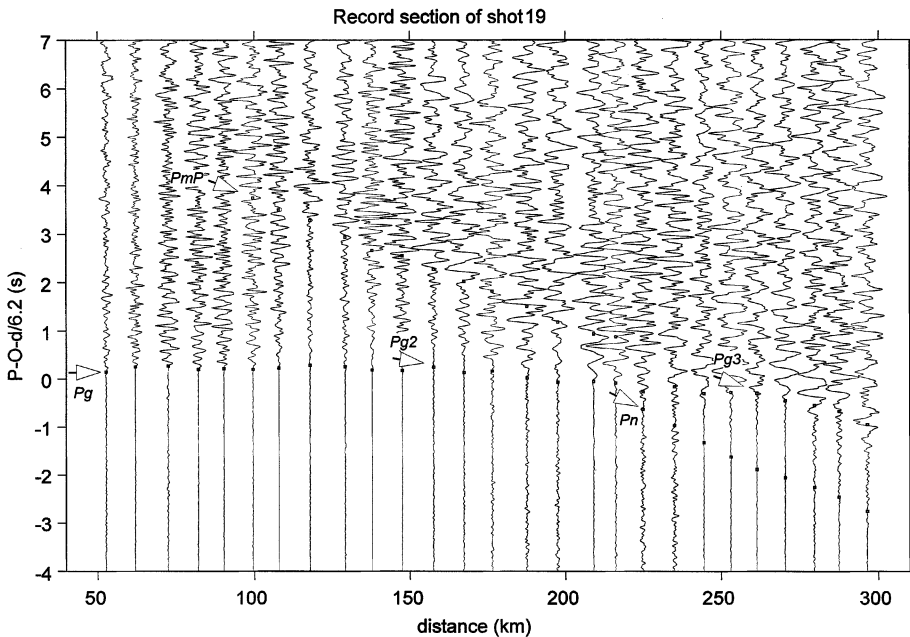

Fig. 10.   *A record section for Shot 19 of the JARE-21 experiment.   Similar to Fig. 3, we applied a reduction velocity of 6.2 km/s.   The onsets of refracted and reflected waves are indicated by small squares.   Pg, Pg2, Pg3 and Pn indicate the refracted arrivals from the upper crust, the middle crust, the lower crust and the Moho boundary, respectively.   PmP indicates the reflected arrivals from the Moho boundary.*

characterized by four branches of arrivals; refracted waves from the crust (*Pg*, *Pg*2 and *Pg*3) and the Moho discontinuity (*Pn*). Prominent reflected waves from the Moho (*PmP*) are also observed. The first branch *Pg* is observed in the distance range of 50–150 km and has an apparent velocity of 6.2 km/s. The second branch *Pg*2 corresponds to the 150–260 km range with an apparent velocity of 6.4 km/s. The third branch *Pg*3 in the distance range of 260–300 km has an apparent velocity of about 6.9 km/s. Moreover, the *Pn* arrivals have an apparent velocity of 7.5 km/s. The four obtained branches suggest that the crust has at least three layers of different velocities.

3.   Method and results for determining *P* velocity model

3.1.   Method

Since six different layer velocities are obtained from the analysis of travel-time, as described above, we assumed a layered model for the crust including an ice sheet. The modeling approach used in this study is a layer stripping method, in which deeper layers are successively determined while keeping the parameters of the predetermined shallower layers fixed. Layer velocity and thickness are determined by ray-tracing forward modeling, combined with travel-time inversion using refraction and wide-angle reflection arrival times. For this calculation, we use the algorithm of Zelt and Smith (1992), a 2-D method which involves numerically solving the ray tracing equations. This algorithm uses a model parameterization based on two types of nodes, depth and velocity. Layer boundaries are created by linearly interpolating a series of depth nodes. Velocity nodes are positioned at the top and bottom of each layer, and the velocity structure within each layer is determined by laterally interpolating the velocity nodes.

As for an initial condition of each layer, apparent velocities were applied to the velocity nodes, where the number and position of nodes were determined by a trial and error method, considering the travel-time misfits. We performed a forward modeling for the first step, then applied travel-time inversion to the resultant model, in order to obtain the optimal values of the boundary depth and the velocity. The main criteria for choosing the final model were minimizing the RMS travel-time residuals and chi-square error misfits while maximizing the number of rays to be traced to the observation points. In other words, the obtained final model should include as many paths from source to receiver as possible on the basis of acceptable travel-time fit.

3.2.   Ice sheet

Table 1 shows the summary of travel-time inversions. The columns indicate (1)

Table 1.   Results of the travel-time inversion.

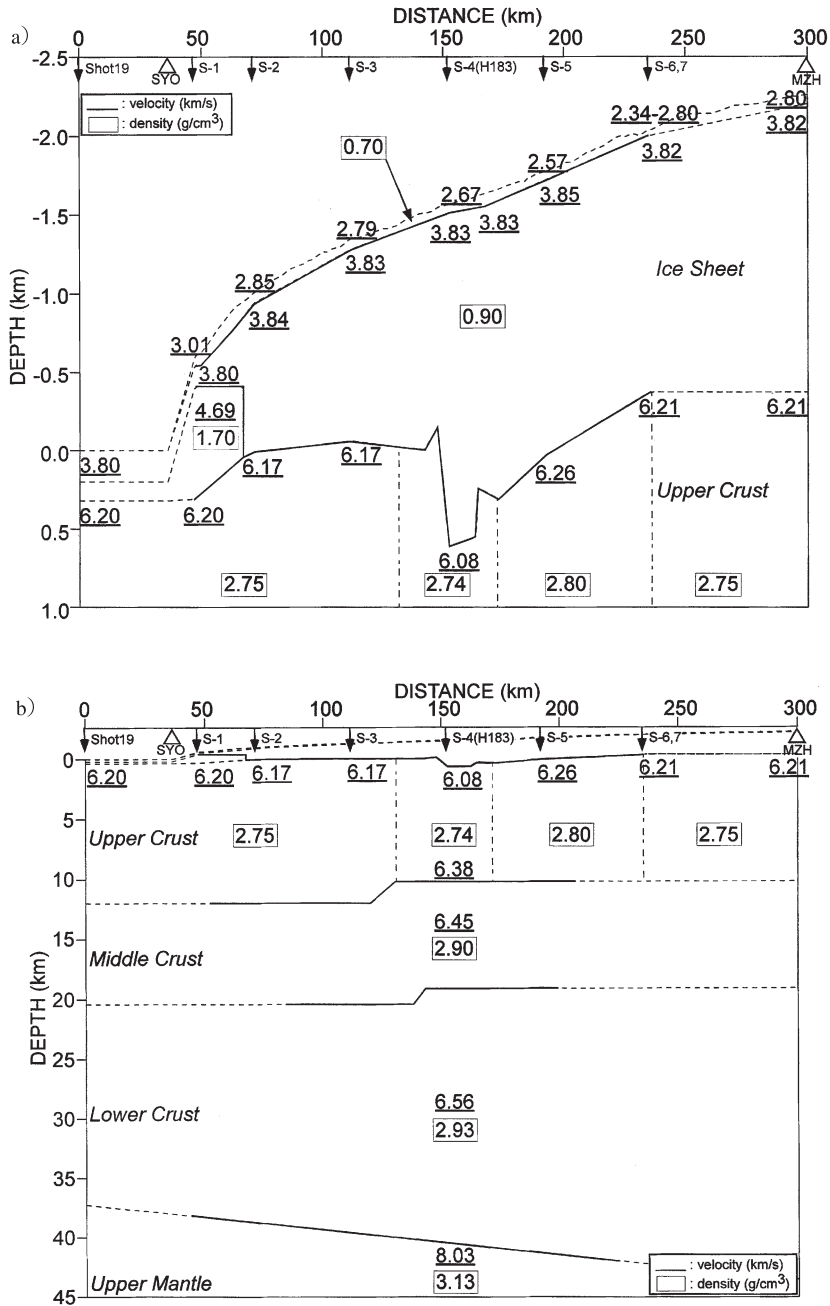|		Number of picks	Number of traced picks	RMS of pickup error (s)	RMS of travel-time residuals (s)	Chi square (s²)
a	Ice sheet	349	349	0.016	0.014	0.790
b	Upper crust	575	548	0.057	0.056	3.701
c	Mid and lower crust	215	213	0.056	0.060	1.502
d	Uppermost mantle	120	119	0.070	0.091	3.865

Fig. 4. Finally obtained model of (a) the ice sheet and the uppermost crust and (b) the entire crust and the uppermost mantle. The shot points in Fig. 4 are indicated by arrows. Dashed lines show the ice sheet surface. Solid lines show the estimated layer boundaries which are covered by the synthetic ray paths. Velocities are shown by numerals with underline in km/s. The densities are given in g/cm³ within a box. The abscissa shows the distance from Shot 3.
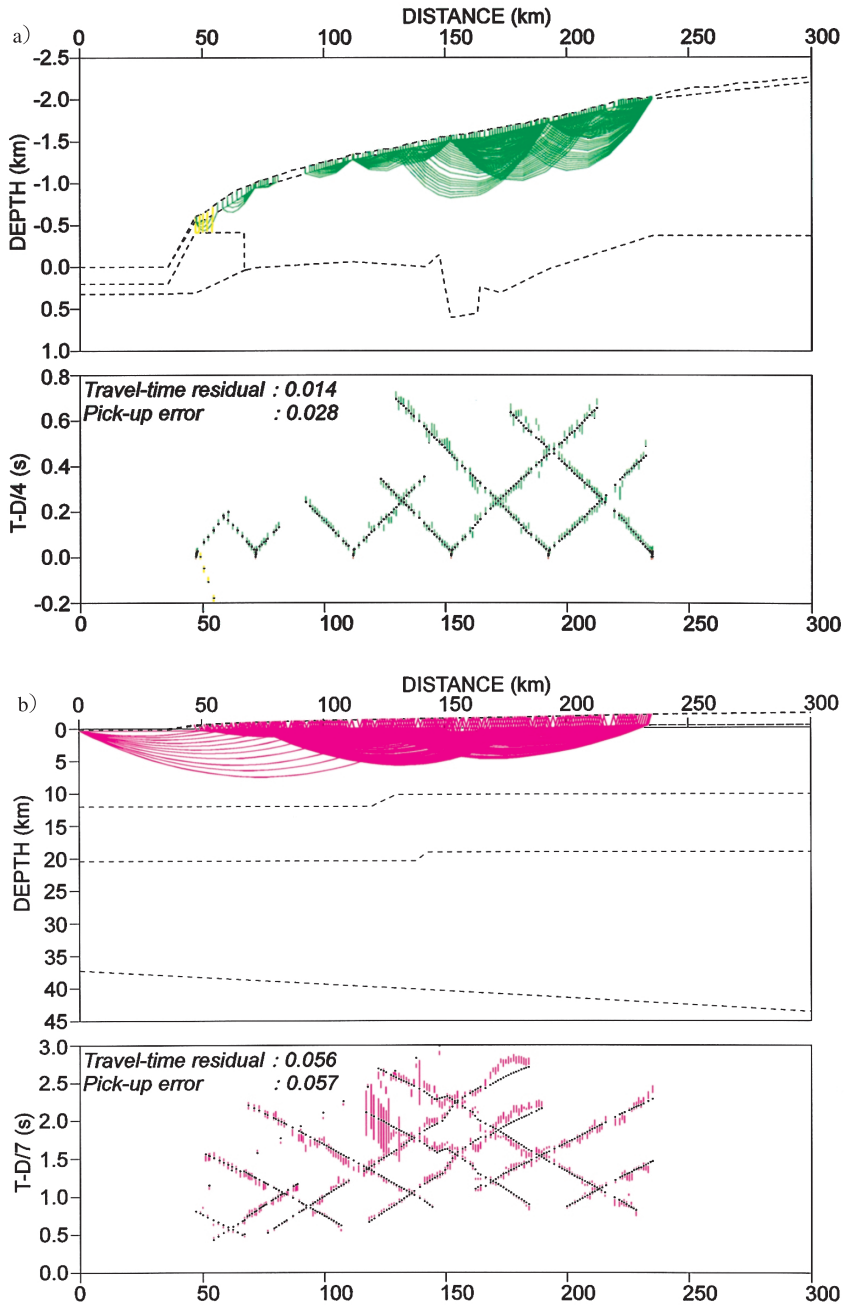
Fig. 7. Ray path diagram (upper panel) and travel-time comparison (lower panel) for the final model; (a) structure of ice sheet, (b) uppermost crust, (c) upper and middle crust, and (d) lower crust and uppermost mantle. Layer boundaries are indicated by dashed lines and arrows show the shot points. Comparison of calculated (dot) and observed travel-times (color bars) is given in the lower panel. The uncertainty of the observed travel-times proportional to the length of the bar. The abscissa shows the distance from Shot 3.
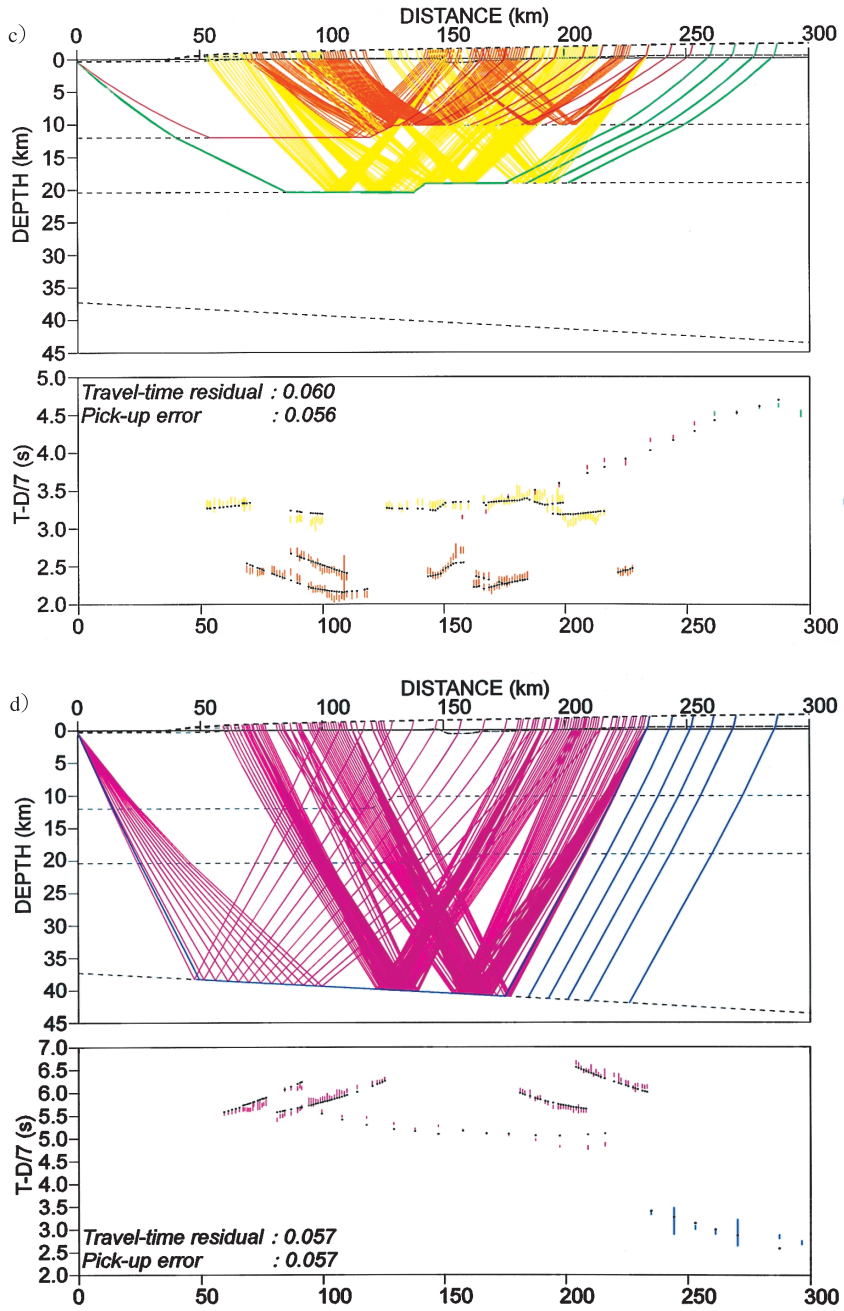
Fig. (Continued).

the number of onsets, (2) the number of traced rays, (3) RMS errors in picking up arrival time, (4) travel-time residuals and (5) chi-square.   The resultant model is shown in Fig. 11a.   The model well explains the observed travel-times, row (a) of Table 1, because the RMS of travel-time residuals (0.014 s) and the RMS error of arrival times (0.016 s) are small and almost equivalent.

The structure of the ice sheet is obtained from refracted waves of the JARE-41 data set and the ray paths traced from sources to stations are shown in Fig. 12a.   Travel-time fittings between observed arrivals and calculated arrivals are very good, as shown in the bottom panel of the Fig. 12a.   The deepest point of the ice sheet refraction is about half of the thickness at most, so the velocity from the middle to the deeper part cannot be determined from the first arrivals.

As shown in the preceding chapter, the velocity increase is continuous but steep near the surface in the ice sheet.   However, travel times in the ice sheet are well approximated by two layers as shown in Fig. 9.   An additional layer with a velocity of 4.69 km/s is added near the coast, considering the apparent velocity of 4.7 km/s derived from the S-1 shot.   The ice sheet has a 60–100 m thin surface layer with P-wave velocities ranging from 2.34 to 3.01 km/s, which vary laterally from place to place. The dominant part of the ice sheet under the surface layer has a P-wave velocity of 3.80–3.85 km/s, which is obtained from the travel-time analysis, including the rays from the basement layer, as shown in Fig. 12b.   The nearly constant velocity in the second layer of the ice sheet explains the travel times well.   This shows that the velocity gradient is very small in the second layer of the ice sheet.   A block with an apparent velocity of 4.7 km/s, existing only under the shot S-1 area, is shown to have a boundary at 410 m above sea level.

3.3.   Crust

Rows (b) and (c) in Table 1 show the summary of travel time inversions for the three-layer crust; the obtained final model is shown in Fig. 11b.   The rays and travel-times are indicated in Figs. 12b and 12c.

The uppermost part of the crust is constructed from direct waves of JARE-41 and JARE-21 data sets, of which the ray path is shown in the upper panel in Fig. 12b.   On the other hand the deeper parts are determined both from refractions in the JARE-21 data set and wide-angle reflections in the JARE-41 data set.   The ray paths in Fig. 12c show reflected waves and head waves from the boundary of the upper and middle crust (orange), head waves through the same boundary (red), reflected waves from the boundary of the middle and lower crust (blue) and head waves through the same boundary (green), for the JARE-21 and JARE-41 experiments.

The synthetic travel times for the model fit the observed ones well as shown in Figs. 12b and 12c.   In addition, the RMS travel-time residual and the RMS pick up error of observed arrival times are small, about 0.05–0.07 s, and almost the same as each other, as shown in Table 1.   In particular, the uppermost crust (Fig. 12b) with a solid line has high accuracy because of the high density of ray paths.

Depth variations of the boundary between the ice sheet and the uppermost crust are large.   They include a 600 m v-shaped valley under the shot S-4 (Fig. 11).   The velocity at the top of this layer varies along the boundaries, that is, 6.17–6.20 km/s on

the ocean side from the valley, 6.08 km/s in the valley and 6.21–6.26 km/s on the inland side (Fig. 11a).   The bottom velocity of this layer is found unchanged, as 6.38 km/s fits the observed travel times (Fig. 11b).

The boundary at the top of the middle crust is generally about 10 km deep and has a 1.8 km step between shot points S-3 and S-4 (Fig. 11b).   The *P*-wave velocity of 6.45 km/s with a small gradient of the layer fits the observed travel times very well.   The boundary at the top of the lower crust is generally 20 km deep and has a 1.3 km step below and near the shot S-4 (Fig. 11b).   The *P*-wave velocity of this layer is 6.56 km/s and is characterized by a small velocity gradient.   However, since the velocity is estimated mainly from the travel-times of one-sided refractions by JARE-21 data and those of reflected waves by JARE-41 data as shown in Fig. 12c, the associated accuracy is not so good as in the upper two layers.   Since rays of refracted waves are not numerous in the middle and in the lower crust, and there are no reversed rays, our model assumes constant velocities in the two layers.   Therefore, velocities have ambiguity of about 0.1–0.2 km/s in the layers, which results in depth errors of the layer boundaries. However, the *Pn* phases constrain the total travel times in the crust; the change in depths of the boundary in the middle and lower crust is less than about 5 km.

3.4.   *Moho boundary*

Row (d) of Table 1 shows the summary of travel-time inversions.   The pink curves shown in Fig. 12d (upper panel) indicate the ray paths of wide-angle reflection observed in JARE-41, while blue ones indicate those of refractions observed in JARE-21.   As shown in the lower panel of Fig. 12d, the adopted velocity model in the upper mantle shown in Fig. 11 explains the observed travel times well.   The RMS of travel-time residuals 0.091 s is roughly comparable with that of picked arrival times (0.080 s) as shown in Table 1 and Fig. 12d.

The depth of the Moho discontinuity is almost 40 km, with a gentle down-slope toward the inland direction, as shown in Figs. 11b or 12d.   The *P*-wave velocity of the uppermost mantle is determined to be 8.03 km/s, with the Moho depth changing from 38 to 42 km along the profile.   As the Moho velocity (*Pn*) is determined from the one-sided first arrivals of JARE-21 data and reflections by JARE-41 data, there is a trade-off between the *Pn* velocity and the dip of the Moho; the dip is relatively small because it is constrained by the reflected waves in the shallower part of the crust.   The apparent velocity of shot 19 is about 8.05–8.1 km/s from the ocean toward the inland direction, so the given true velocity 8.03 km/s gives a dip of about 1 degree.   This shows that the Moho has a gentle dip toward the inland side from the coastal region.

4.   Estimation of *Vp/Vs*

One of the significant features of the JARE-41 data set is that clear *S*-waves are recorded on the vertical component seismograms.   However, since the number of stations with clear *S*-wave onsets are limited, we estimate an approximate *Vp/Vs* value from the trace of S-arrivals or record sections.

Figure 13 shows a band-pass filtered (5–11 Hz) record for the *S*-arrival part of shot S-2, reduced by a velocity of 3.6 km/s.   Observed *S*-wave arrivals fit calculated ones,
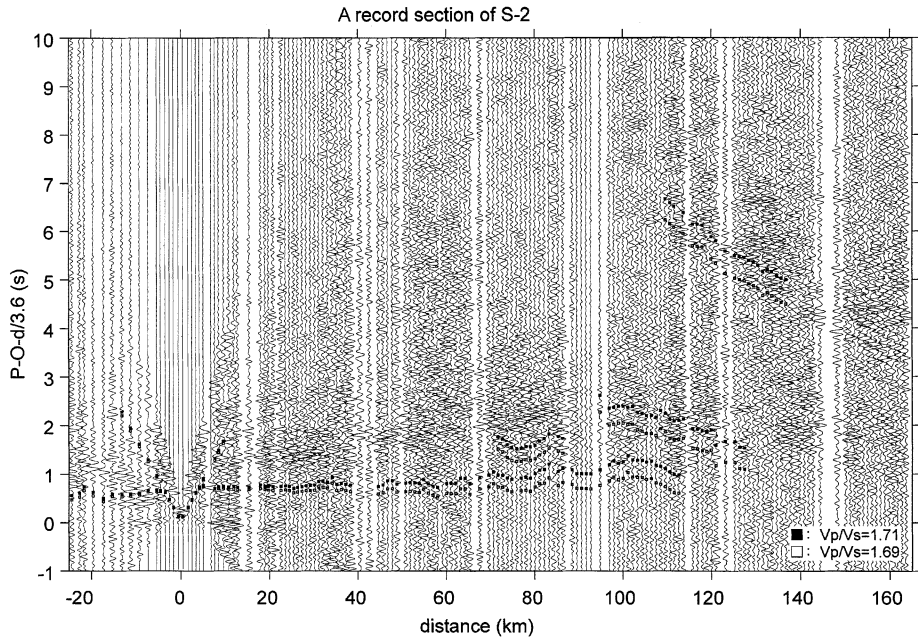
Fig. 13. *A band-pass filtered record (5–11 Hz) for the shot S-2. The abscissa shows the distance from the shot point in km and the ordinate shows the reduced travel time in seconds with a velocity of 3.8 km/s. Calculated S wave arrivals are plotted for the assumed Vp/Vs of 1.69 (open square) and 1.71 (solid squares).*

multiplying P-wave travel-time for the final P-wave model by an assumed Vp/Vs value. The Vp/Vs are assumed to be 1.69 or 1.71 and the synthetic S-wave first and reflected arrivals are plotted on a record section of Fig. 13. A similar procedure is followed for record sections of all other shots. Since the rays of reflected waves penetrate deeper into the crust than the refracted waves as shown in Figs. 12c and 12d, the difference in Vp/Vs in the crust from the assumed value should cause misfits between calculated and observed S-wave travel times. However, adopted Vp/Vs values explain the observed S-wave arrivals well, not only from crustal refractions but also from the Moho reflections for each shot in the JARE-41 experiment. This shows that the Vp/Vs values in the crust are nearly the same, 1.69–1.71.

5. Density structure from gravity data

The JARE-41 seismic party also conducted gravity measurements at all seismic observation sites. The data were corrected for earth tide and instrumental drift referring to the gravity control point of Syowa Station by using the method of Toda *et al*. (2001). We furthermore applied free air and atmospheric gravity corrections based on the Geodetic Reference System 1980, and try to reproduce observed gravity anomalies from the layered density structure model on the basis of the P-wave velocity model derived in the previous sections.

In the density model, the same layer boundaries are taken from obtained velocity structures in Fig. 11. The velocities were compared to density based on laboratory measurements of the relationship between *P*-wave velocities and densities for rocks. Figure 14 shows the *P*-wave velocity versus density diagram for various rocks after Barton (1986) (original data are given in Ludwig *et al.*, 1970). We also added measurements for rock samples in the Lützow-Holm Bay area (Fig. 1), Antarctica, after Yukutake and Ito (1984) and Kitamura *et al.* (2001).
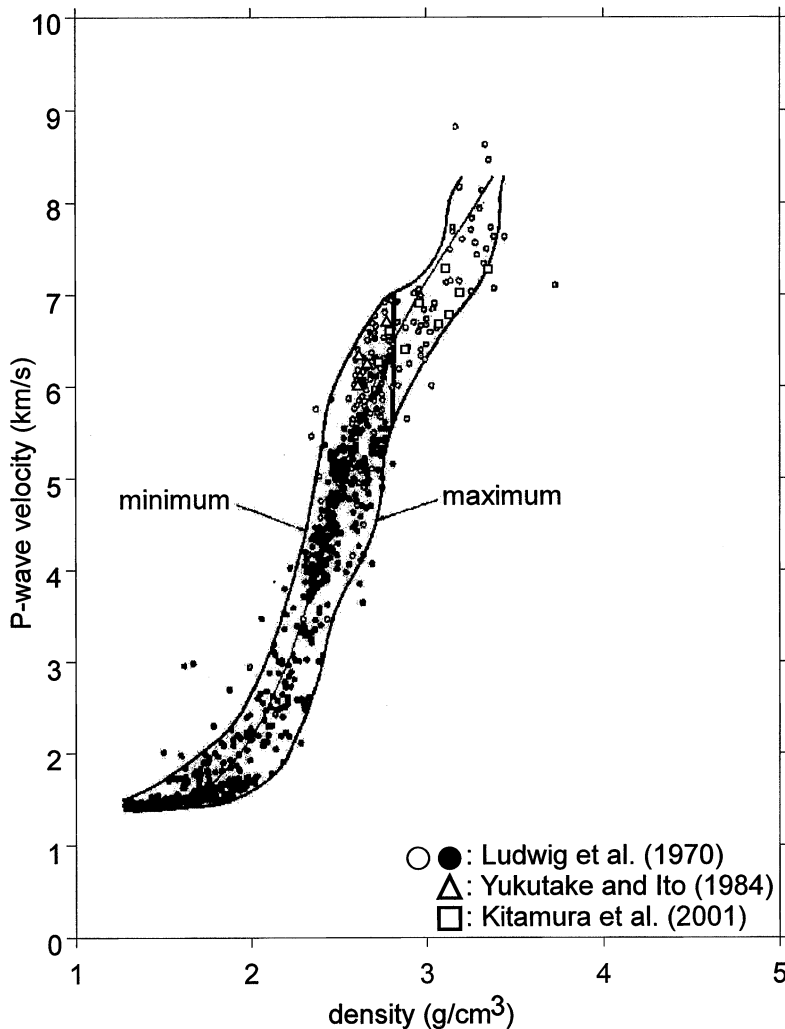

Fig. 14. *Summary of laboratory measurements inferring the relation between the P-wave seismic velocities and rock densities after Barton (1986) (from Ludwig et al., 1970). The thin line between the maximum and minimum density values (heavy lines) indicates the mean velocity-density relationship. Results by Yukutake and Ito (1984) and Kitamura et al. (2001) are added.*
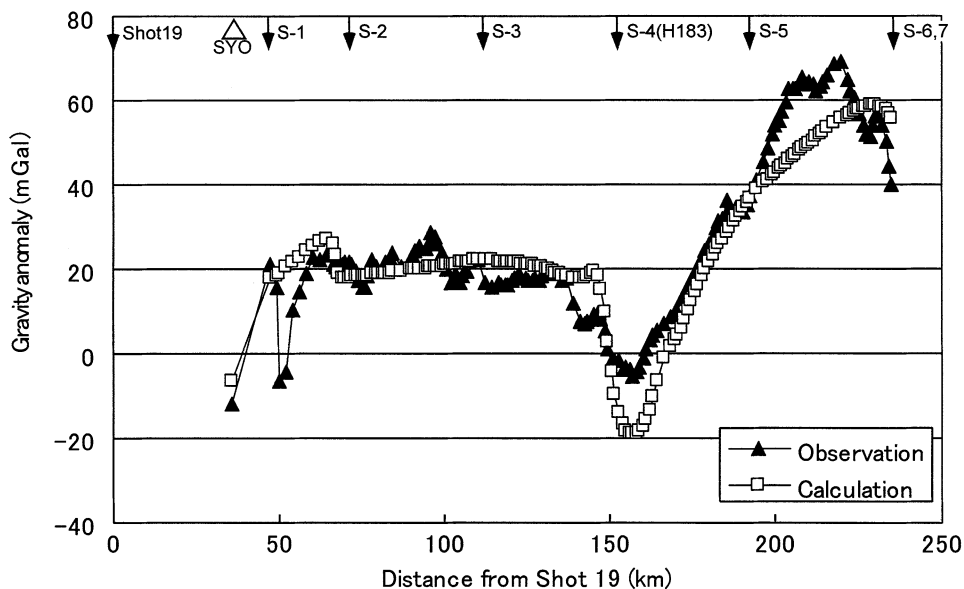
Fig. 15. Calculated gravity anomalies (open squares) by the program of Komazawa (1984, 1995) and observed free-air gravity anomalies (solid triangles). The abscissa shows the distance from Shot 19.

As starting values, the density of the ice sheet is given as $0.9 \, g/m^3$ without using the relationship in Fig. 14. Average values of densities are selected corresponding to P-wave velocities given in Fig. 11 for the upper, middle and lower crustal layers. However, since felsic gneiss is possibly the dominant rock along the Mizuho traverse route as discussed in the next chapter, we take a slightly larger density of around 2.75 g/cm^3 than the average of 2.65 g/cm^3 for the uppermost crust. The averaged densities corresponding to the P-wave velocities of 6.2–6.6 km/s are roughly 2.7–2.9 g/cm^3; the possible range of density is as large as 2.4–3.1 g/cm^3. Therefore, the density-velocity relation is only a reference for the crust. The density values were changed within the ranges, until a good fit between observed and calculated free-air gravity anomalies were obtained by trial-and-error. In the procedure, we applied a program by Komazawa (1984, 1995) to calculate the synthetic gravity anomalies. The best density model we obtained is shown in Figs. 11a and 11b. The observed (solid triangle) free-air gravity anomalies in Fig. 15 are almost coincident with the synthetic ones (open squares), although there are some misfits in the valley of basement rock and around shot-points S-1 and S-6.

6. Discussion

6.1. *Valley of the basement rock and low velocity*

The relatively 0.1 km/s low velocity of 6.08 km/s is obtained in the valley-shaped basement under shot point S-4. We examined the significance of this value. When we

searched the most optimal model by fixing the uppermost crustal velocity at 6.2 km/s, systematic travel-time misfits between the observation and the synthetic calculation along the profile line were obtained. On the other hand, the RMS of travel-time residuals is equivalent to that of the final model. Therefore, we conclude that the final model is better than the model with a constant velocity.

From the gravity analysis in Section 5, a synthetic density model based on a velocity structure was shown to have misfits to the observed gravity around this area, suggesting higher density materials than ice. Low velocity sediments with higher density than ice or a mixture of ice with sand or stones are candidates for the composition at the bottom of this valley. Furthermore, the JARE-43 seismic profile crossed the JARE-41 profile over this valley, and Miyamachi *et al*. (2003) derived a valley shaped basement with about 600 m depth in the same location. So it is suggested that the general form of the basement of this area is like a crater. In addition, since the velocity of the basement is about 0.1 km/s lower than those at both sides of the observation line, it could be of different rock type. The misfits of the gravity data, relatively higher gravity anomalies and the low velocity may be explained by the existence of volcanic sediments at the
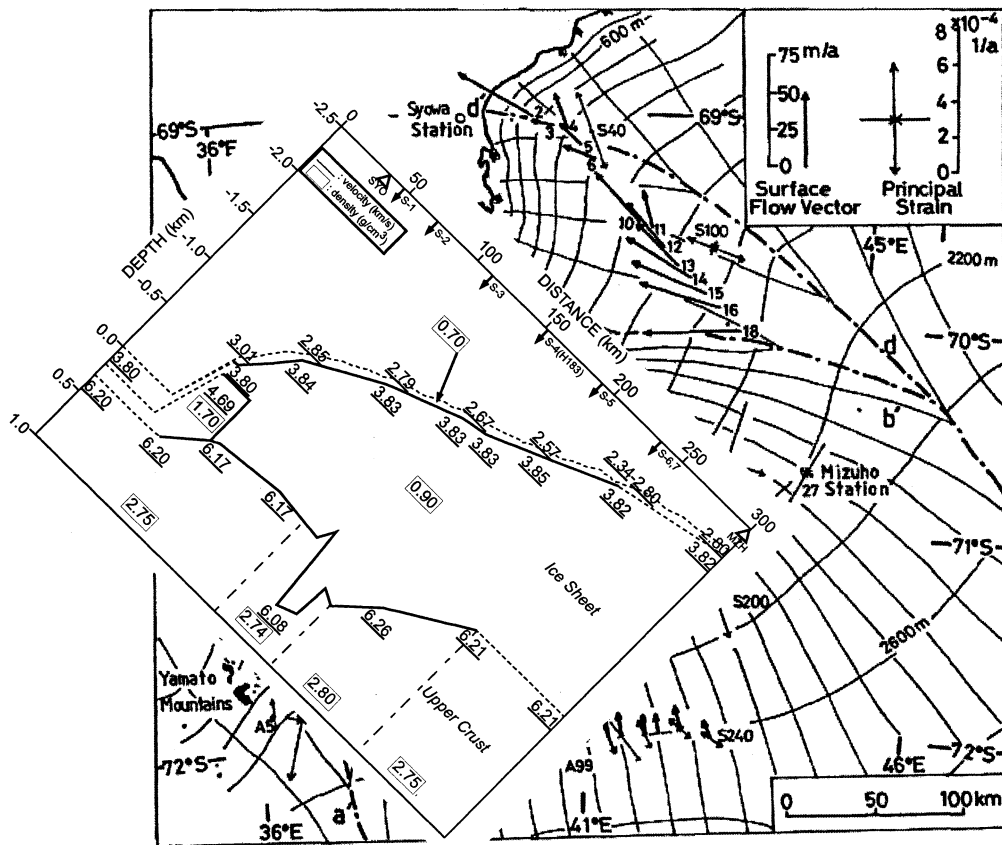

Fig. 16. Ice sheet flow after Shibuya and Ito (1983). Figure 11 is superposed for comparison.

bottom of the valley and magmatic intrusions, respectively.

JARE-14 carried out a traverse survey along the Mizuho route by installing 109 traverse poles.   Most of the JARE-21 seismic stations were selected to be close to the JARE-14 traverse stations.   By comparing the positions of the JARE-21 stations with the JARE-14 traverse stations, the flow velocity of the ice sheet along the Mizuho traverse route was estimated (Shibuya and Ito, 1983).   In Fig. 16, the flow vectors are represented together with the velocity model obtained as in Fig. 11.   The valley of this basement structure corresponds to the point where flow direction changes.   The flow directions are along the Mizuho route toward the ocean from the valley and change by 30 degrees farther inland.   The obtained velocity model is consistent with the change in flow direction of the ice sheet and also the topography of the ice sheet surface.

6.2.   Comparison with previous models

Tsutsui et al. (2001a) obtained the P-wave velocity structure of the ice sheet and the shallow crust by the method of difference (Hagiwara, 1938) using the JARE-41 data set.   However, the basement shape under the shot point S-4 could not be determined because a step change of ice thickness violated the assumption of the analysis method. The boundary depths between the ice sheet and the basement of other parts of the profile by Tsutsui et al. (2001a) are almost the same as those in this study.   The velocity value of the basement rock layer by Tsutsui et al. (2001a) is 6.2 km/s, except near the shot point S-1, where the velocity 5.2 km/s is obtained.   In our final model, the basement rock velocities slightly varied; 6.17–6.20 km/s on the ocean side, 6.08 km/s under the valley near shot point S-4 and 6.21–6.26 km/s on the inland side.   As for a 4.7 km/s local block between the ice sheet and basement in the area of shot point S-1 to near S-2 in our study, this corresponds to the basement velocity of 5.2 km/s by Tsutsui et al. (2001a).   The difference seems to have resulted from the treatment of Px arrivals. Tsutsui et al. (2001a) considered it to be the refractions from the basement, but we consider it to be from some kind of sedimentary layer, because the velocity of 4.7 km/s is too fast for the ice sheet while the converted density of about 2.3 g/cm^3 in Fig. 14 is too small for rocks.   We consider that this 4.7 km/s layer could be a mixture of ice with sands or stones.

Ikami et al. (1984) obtained crustal structure using the data set of the JARE-21 experiment.   As for the model by Ikami et al. (1984), the uppermost crust consists of a 3-layer crust having P-wave velocities of 6.0, 6.3, and 6.8–6.9, with thicknesses of 3–4, 22–25 and 10–15 km, respectively.   On the other hand, our model has a P-wave velocity of about 6.2 km/s in the upper crust and 6.56 km/s in the lower crust as shown in Fig. 11b.   The velocity structure in Ikami et al. (1984) has an upper crust of relatively low velocity; the lower crust of relatively high velocity compares with the velocities in our model.   In this study, the upper crustal structures are well-constrained by refractions because the numbers of rays used in this study are much larger than in the previous model, and our results greatly improve the crustal structure along the Mizuho route.   It is difficult to fit the observed travel times to the travel times calculated from the model in Ikami et al. (1984).   The approximate depth of the Moho discontinuity is about the same as that by Ikami et al. (1984), but our model indicates a gentle dip toward the inland direction.

6.3. Implications of the model for rock types of the crust

Figure 17 shows plots of *P*-wave velocity against Poisson's ratio for (a) mid crustal and (b) lower crustal rock types in the results of laboratory measurements by Holbrook *et al.* (1992).   A solid triangle, an open triangle and an inverted open triangle correspond to our results for the upper crust (6.1–6.3 km/s), the middle crust (6.45 km/s) and the lower crust (6.56 km/s), respectively.   From Fig. 17, granite, felsic amphibolite facies gneiss and quartz-mica schist may correspond to the composition in the upper crust.

The Mizuho Plateau located on the Lützow-Holm Complex (LHC), had experienced regional metamorphism in the early Paleozoic, as part of the Pan-African orogeny (*e.g.*, Shiraishi *et al.*, 1994).   The metamorphic grade increases progressively from the Prince Olav Coast to the Sôya Coast; and the maximum thermal axis lies in southern Lützow-Holm Bay with a NNW-SSE orientation (Hiroi *et al.*, 1991; Motoyoshi *et al.*, 1989).   The LHC was deformed under compression stress perpendicular to the thermal axis during the Pan-African metamorphism.   The transitional zone between amphibolite facies and granulite facies along the western part of the Prince Olav Coast is defined by the first appearance of orthopyroxene in ordinary basic to felsic/intermediate gneisses.
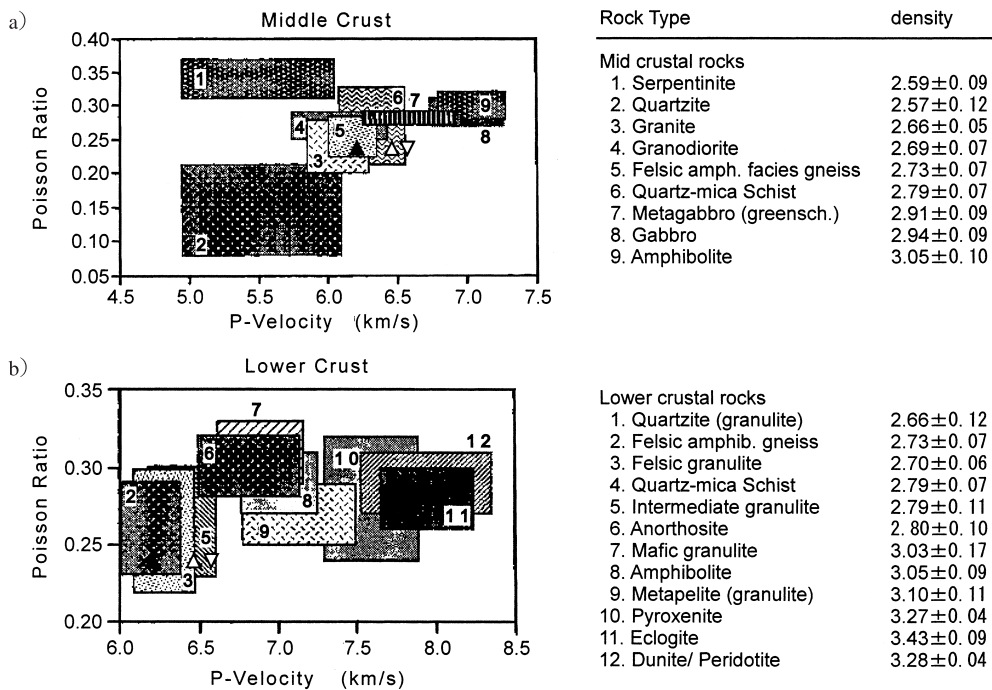

Rock Type	density
Mid crustal rocks	
1. Serpentinite	2.59±0. 09
2. Quartzite	2.57±0. 12
3. Granite	2.66±0. 05
4. Granodiorite	2.69±0. 07
5. Felsic amph. facies gneiss	2.73±0. 07
6. Quartz-mica Schist	2.79±0. 07
7. Metagabbro (greensch.)	2.91±0. 09
8. Gabbro	2.94±0. 09
9. Amphibolite	3.05±0. 10

Rock Type	density
Lower crustal rocks	
1. Quartzite (granulite)	2.66±0. 12
2. Felsic amphib. gneiss	2.73±0. 07
3. Felsic granulite	2.70±0. 06
4. Quartz-mica Schist	2.79±0. 07
5. Intermediate granulite	2.79±0. 11
6. Anorthosite	2. 80±0. 10
7. Mafic granulite	3.03±0. 17
8. Amphibolite	3.05±0. 09
9. Metapelite (granulite)	3.10±0. 11
10. Pyroxenite	3.27±0. 04
11. Eclogite	3.43±0. 09
12. Dunite/ Peridotite	3.28±0. 04

Fig. 17.   Plots of P-velocity vs. Poisson's ratio for the rock types composing (a) the mid crust and (b) the lower crust, from laboratory measurements after Holbrook et al. (1992).   The results in this study are plotted by a solid triangle (upper crust), an open triangle (middle crust) and an inverted open triangle (lower crust), respectively.

Comparing our seismic velocities with those from laboratory measurements, felsic gneiss could be the dominant component of the upper crust beneath Mizuho Plateau. On the contrary, quartz-mica schist, felsic granulite and intermediate granulite have possibilities to be the composition in the middle and lower crust from Fig. 17. It is difficult, however, to infer the composition of the deeper crust because there is little information on the physical properties. However, we speculate that deeper crust in the surveyed area is not so mafic.

7. Summary

A P-wave velocity model from the ice sheet to the uppermost mantle is derived by ray-tracing travel-time analysis for the refractions and wide-angle reflections in the Mizuho Plateau. The obtained features of this model are summarized as follows: (1) The ice sheet has a 60–100 m thick surface layer with P-wave velocity of 2.34–3.01 km/s, and the dominant deeper layer has a P-wave velocity of 3.80–3.85 km/s. (2) There is a valley with a drop of 600 m in the basement topography in the middle of the profile around the shot point S-4, which is consistent with the variations of ice sheet flow. (3) The uppermost crust has a P-wave velocity of 6.17–6.20 km/s on the coastal side, 6.08 km/s under the valley described above and 6.21–6.26 km/s on the inland side. (4) The middle and the lower crustal P-wave velocities are 6.45 and 6.56 km/s, and the thicknesses are about 10 and 20 km, respectively. (5) The Moho with a P-wave velocity of the uppermost mantle of 8.03 km/s is almost 40 km deep with a gentle dip toward the inland direction. (6) The Vp/Vs value of the entire crust is about 1.70 from the S-wave analysis. (7) Gravity anomalies calculated with the density structure based on the obtained velocity structure explain the observed ones well, but there are some misfits at the valley of the basement and around shot points S-1 and S-6.

From these results, we have speculated with respect to the rock composition in the shallow crust as follows: (1) Felsic gneiss is possibly the dominant rock in the uppermost crust under the Mizuho traverse routes. (2) The block with a 4.69 km/s P-wave velocity near the coast area may be mixture of ice with sand or stones. (3) Low velocity sediments or the above mixture may be accumulated in the bottom of the valley under shot point S-4.

of Dr. Komazawa (AIST) are also used for the gravity analysis.

References

Barton, P.J. (1986): The relationship between seismic velocity and density in the continental crust - a useful constraint? Geophys. J. R. Astr. Soc., **87**, 195–208.

Eto, T. (1971): Seismic studies during the JARE South Pole traverse 1968–69. JARE Sci. Rep., Spec. Issue, **2**, 115–124.

Hagiwara, T. (1938): A method for travel time analysis in case layer boundaries are not uniform. Jishin Series I, **10**, 463–468 (in Japanese).

Harley, S. and Hansen, B.J. (1990): Archean and Proterozoic high-grade terraces of East Antarctic Shield (40°–80°E): a case study of diversity in granulite facilities. High-Temperature Metamorphism and Crustal Anatexis, ed. by J.R. Ashworth and M. Brown. London, Unwin Hyman, 320–370 (The Mineralogical Society Series 2).

Hiroi, Y., Shiraishi, K. and Motoyoshi, Y. (1991): Late Proterozoic paired metamorphic complexes in East Antarctica, with special reference to the tectonic significance of ultramafic rocks. Geological Evolution of Antarctica, ed. by M.R.A. Thomson *et al*. Cambridge, Cambridge Univ. Press, 83–87.

Holbrook, W.S., Mooney, W.D. and Christensen, N.I. (1992): The seismic velocity structure of the deep continental crust. Continental Lower Crust, ed. by D.M. Fountain *et al*. Amsterdam, Elsevier, 1–43.

Ikami, A., Ito, K., Shibuya, K. and Kaminuma, K. (1984): Deep crustal structure along the profile between Syowa and Mizuho Stations, East Antarctica. Mem. Natl Inst. Polar Res., Ser. C (Earth Sci.), **15**, 19–28.

Ito, K., Ikami, A., Shibuya, K., Kaminuma, K. and Kataoka, S. (1983): Field operation of explosion seismic experiment in Antarctica (Second Paper). Nankyoku Shiryô (Antarct. Rec.), **79**, 107–133 (in Japanese with English abstract).

Kitamura, K., Ishikawa, M., Arima, M. and Shiraishi, K. (2001): Laboratory measurements of *P*-wave velocity of granulites from Lützow-Holm Complex, East Antarctica: Preliminary report. Polar Geosci., **14**, 180–194.

Komazawa, M. (1984): On the quantitative gravimetric analysis in the Hokuroku District. Butsuri Tankô (Geophysical Exploration), **37** (3), 19–45 (in Japanese with English abstract).

Komazawa, M. (1995): Gravimetric analysis of Aso Volcano and its interpretation. J. Geod. Soc. Jpn., **41** (1), 17–45.

Lawver, L.A., Gahagan, L.M. and Dalziel, I.W.D. (1998): A tight fit-early mesozoic Gondwana, A plate reconstruction perspective. Mem. Natl Inst. Polar Res., Spec. Issue, **53**, 214–229.

Ludwig, J.W., Nafe, J.E. and Drake, C.L. (1970): Seismic refraction. The Sea, Vol. 4, ed. by A.E. Maxwell. New York, Wiley, 53–84.

Miyamachi, H., Murakami, H., Tsutsui, T., Toda, S., Minta, T. and Yanagisawa, M. (2001): A seismic refraction experiment in 2000 on the Mizuho Plateau, East Antarctica (JARE-41)—Outline of observations—. Nankyoku Shiryô (Antarct. Rec.), **45**, 101–147 (in Japanese with English abstract).

Miyamachi, H., Toda, S., Matsushima, T., Takada, M., Takahashi, Y., Kamiya, D., Watanabe, A., Yamashita, M. and Yanagisawa, M. (2003): A seismic refraction and wide-angle reflection exploration in 2002 on the Mizuho Plateau, East Antarctica—outline of observations (JARE-43)—. Nankyoku Shiryô (Antarct. Rec.), **47**, 32–71 (in Japanese with English abstract).

Motoyoshi, Y., Matsubara, S. and Matsueda, H. (1989): *P-T* evolution of the granulite-facies rocks of the Lützow-Holm Bay region, East Antarctica. Evolution of Metamorphic Belts, ed. by J.S. Daly *et al*. London, Geol. Soc., 325–329 (Geol. Soc. Spec. Issue, **43**).

Narita, H., Maeno, N. and Nakawo, M. (1978): Structural characteristics of firn ice cores drilled at Mizuho Station, East Antarctica. Mem. Natl Inst. Polar Res., Spec. Issue, **10**, 48–61.

Shibuya, K. and Ito, K. (1983): On the flow velocity of the ice sheet along the traverse route from Syowa to Mizuho Stations, East Antarctica. Mem. Natl Inst. Polar Res., Spec. Issue, **28**, 260–276.

Shibuya, K. and Kaminuma, K. (1982): Utilization of an NNSS receiver in the explosion seismic experiments on the Prince Olav Coast, East Antarctica, 1. Recovered UTC. Nankyoku Shiryô (Antarct. Rec.),

76, 63–72.

Shibuya, K., Ito, K. and Kaminuma, K. (1982): Utilization of an NNSS receiver in the explosion seismic experiments on the Prince Olav Coast, East Antarctica, 2. Positioning. Nankyoku Shiryô (Antarct. Rec.), **76**, 73–88.

Shiraishi, K., Ellis, D.J., Hiroi, Y., Fanning, C.M., Motoyoshi, Y. and Nakai, Y. (1994): Cambrian orogenic belt in East Antarctica and Sri Lanka: implication for Gondwana assembly. J. Geol., **102**, 47–65.

Toda, S., Tsutsui, T., Miyamachi, H., Matsushima, T., Kanao, M. and Fukuda, Y. (2001): A high resolution crustal structure on the Mizuho Plateau, East Antarctica, revealed by high density seismic and gravity exploration. The 21st Symposium on Antarctic Geosciences Program and Abstracts, October 2001. Tokyo, Natl Inst. Polar Res., 53.

Tsutsui, T., Murakami, H., Miyamachi, H., Toda, S. and Kanao, M. (2001a): P-wave velocity structure of the ice sheet and the shallow crust beneath the Mizuho traverse route, East Antarctica, from seismic refraction analysis. Polar Geosci., **14**, 195–211.

Tsutsui, T., Yamashita, M., Murakami, H., Miyamachi, H., Toda, S. and Kanao, M. (2001b): Reflection profiling and velocity structure beneath Mizuho traverse route, East Antarctica. Polar Geosci., **14**, 212–225.

Wessel, P. and Smith, W.H.F. (1995): New version of the Generic Mapping Tools released. EOS Trans. Am. Geophys. Union, **76**, 329.

Yamashita, M., Kanao, M. and Tsutsui, T. (2002): Characteristics of the Moho as revealed from explosion seismic reflections beneath the Mizuho Plateau, East Antarctica. Polar Geosci., **15**, 89–103.

Yukutake, H. and Ito, K. (1984): Velocities of P and S waves for drilling core rocks at Syowa Station, Antarctica. Mem. Natl Inst. Polar Res., Spec. Issue, **33**, 17–27.

Zelt, C.A. and Smith, R.B. (1992): Seismic traveltime inversion for 2-D crustal velocity structure. Geophys. J. Int., **108**, 16–34.